



Swansea University  
Prifysgol Abertawe



## Cronfa - Swansea University Open Access Repository

---

This is an author produced version of a paper published in:

*Small*

Cronfa URL for this paper:

<http://cronfa.swan.ac.uk/Record/cronfa41037>

---

### **Paper:**

Ridolfo, R., Ede, B., Diamanti, P., White, P., Perriman, A., van Hest, J., Blair, A. & Williams, D. (2018).

Biodegradable, Drug-Loaded Nanovectors via Direct Hydration as a New Platform for Cancer Therapeutics. *Small*, 14 (32), 1703774

<http://dx.doi.org/10.1002/sml.201703774>

This is an open access article under the terms of the Creative Commons Attribution License.

---

This item is brought to you by Swansea University. Any person downloading material is agreeing to abide by the terms of the repository licence. Copies of full text items may be used or reproduced in any format or medium, without prior permission for personal research or study, educational or non-commercial purposes only. The copyright for any work remains with the original author unless otherwise specified. The full-text must not be sold in any format or medium without the formal permission of the copyright holder.

Permission for multiple reproductions should be obtained from the original author.

Authors are personally responsible for adhering to copyright and publisher restrictions when uploading content to the repository.

<http://www.swansea.ac.uk/library/researchsupport/ris-support/>

# Biodegradable, Drug-Loaded Nanovectors via Direct Hydration as a New Platform for Cancer Therapeutics

Roxane Ridolfo, Benjamin C. Ede, Paraskevi Diamanti, Paul B. White, Adam W. Perriman, Jan C. M. van Hest,\* Allison Blair,\* and David S. Williams\*

The stabilization and transport of low-solubility drugs, by encapsulation in nanoscopic delivery vectors (nanovectors), is a key paradigm in nanomedicine. However, the problems of carrier toxicity, specificity, and producibility create a bottleneck in the development of new nanomedical technologies. Copolymeric nanoparticles are an excellent platform for nanovector engineering due to their structural versatility; however, conventional fabrication processes rely upon harmful chemicals that necessitate purification. In engineering a more robust (copolymeric) nanovector platform, it is necessary to reconsider the entire process from copolymer synthesis through self-assembly and functionalization. To this end, a process is developed whereby biodegradable copolymers of poly(ethylene glycol)-*block*-poly(trimethylene carbonate), synthesized via organocatalyzed ring-opening polymerization, undergo assembly into highly uniform, drug-loaded micelles without the use of harmful solvents or the need for purification. The direct hydration methodology, employing oligo(ethylene glycol) as a nontoxic dispersant, facilitates rapid preparation of pristine, drug-loaded nanovectors that require no further processing. This method is robust, fast, and scalable. Utilizing parthenolide, an exciting candidate for treatment of acute lymphoblastic leukemia (ALL), discrete nanovectors are generated that show strikingly low carrier toxicity and high levels of specific therapeutic efficacy against primary ALL cells (as compared to normal hematopoietic cells).

therapeutic nanovectors there are, however, a number of issues that cause contention: (1) the use of harmful substances in the fabrication process, (2) elucidating the exact physicochemical nature of the resulting nanostructure, and (3) identifying the key physical features that determine biochemical performance.<sup>[1–6]</sup> Addressing these issues is especially pertinent because so many nanomedical formulations fail to reach the clinic due to unforeseen complications.<sup>[7]</sup> For this reason, structures generated by the self-assembly of amphiphilic block copolymers have received much attention due to their excellent versatility and physical properties.<sup>[8–14]</sup> In particular, the implementation of biodegradable copolymers comprising polyesters and polycarbonates, in combination with poly(ethylene glycol) (PEG), has received increasing attention due to their biocompatibility.<sup>[15–18]</sup> However, typical approaches to their synthesis and fabrication can be greatly improved, in order to decrease reliance upon potentially toxic catalysts and organic solvents. Moreover, it is critically important to have an accurate


picture of the size and shape of the drug nanovectors so that performance in vitro and in vivo can be concisely related to these parameters.<sup>[19–27]</sup>

In particular, the ubiquity of harmful solvents and complex methodologies in the fabrication of drug-loaded delivery vectors

## 1. Introduction

Nanomedicine has gained much interest over the years because of its great potential to transport fragile, toxic, and poorly soluble drugs to the desired sites in the body. In the development of

R. Ridolfo, Prof. J. C. M. van Hest, Dr. D. S. Williams  
Biomedical Engineering  
Eindhoven University of Technology  
P.O. Box 513, 5600 MB Eindhoven, The Netherlands  
E-mail: j.c.m.v.hest@tue.nl; d.s.williams@swansea.ac.uk  
B. C. Ede, Dr. P. Diamanti, Dr. A. W. Perriman, Dr. A. Blair  
School of Cellular and Molecular Medicine  
University of Bristol  
Bristol BS8 1TD, UK  
E-mail: allison.blair@bristol.ac.uk

 The ORCID identification number(s) for the author(s) of this article can be found under <https://doi.org/10.1002/sml.201703774>.

© 2018 The Authors. Published by WILEY-VCH Verlag GmbH & Co. KGaA, Weinheim. This is an open access article under the terms of the Creative Commons Attribution License, which permits use, distribution and reproduction in any medium, provided the original work is properly cited.

DOI: 10.1002/sml.201703774

Dr. P. Diamanti, Dr. A. Blair  
Bristol Institute for Transfusion Sciences  
NHS Blood and Transplant  
Bristol BS34 7QH, UK

Dr. P. B. White  
Institute for Molecules and Materials  
Radboud University  
6525 AJ Nijmegen, The Netherlands

Dr. D. S. Williams  
Department of Chemistry  
Swansea University  
Swansea SA2 8PP, UK

for cancer therapeutics is rarely brought into contention due to the absence of alternative strategies. Recently, direct hydration, which utilizes oligo(ethylene glycol) (OEG) as a nontoxic dispersant, has been presented as an alternative strategy for the aqueous self-assembly of polymeric nanostructures.<sup>[28,29]</sup> Implementation of direct hydration in the fabrication of drug-loaded nanovectors could reduce dependence upon harmful solvents and provide a facile alternative to conventional methodologies. Given the ability of OEG to dissolve certain amphiphilic copolymers and facilitate their dispersion and self-assembly, we postulate that this approach would also be amenable to the generation of drug nanocarriers. However, the application of this alternative methodology toward drug encapsulation and its ability to produce well-defined composite nanovectors, at sizes under 100 nm, is not known. To this end we have explored the use of the biodegradable copolymer poly(ethylene glycol)-block-poly(trimethylene carbonate) (PEG-PTMC) as a potential candidate for direct hydration. PTMC, which has established biodegradability,<sup>[30]</sup> and can be readily prepared using the nontoxic catalyst, methanesulfonic acid,<sup>[31,32]</sup> has been identified as an excellent candidate for drug delivery applications.<sup>[33,34]</sup> In this way, we can also use molecular design to engineer the structural features of copolymeric nanovectors, such as size, if the direct hydration process is amenable to such control.

The therapeutic context for this work is acute lymphoblastic leukemia (ALL), a challenging application that can directly benefit from development of more efficacious treatments. ALL is the most common childhood cancer.<sup>[35–37]</sup> Survival rates, whilst markedly improved over the last 30 years, have started to plateau and treatment-related toxicity has increased.<sup>[38]</sup> There has been little progress in the introduction of new agents over the past decade, largely due to the fact that hydrophobic drug candidates require dissolution in harmful organic solvents and attempts at chemical modification only tend to reduce therapeutic efficacy.<sup>[39,40]</sup> One such drug candidate, the sesquiterpene lactone parthenolide (PTL), has shown promising therapeutic efficacy against ALL with specificity against diseased cells over healthy blood cells.<sup>[40–43]</sup> PTL is a potent NF- $\kappa$ B inhibitor and, as such, has wide ranging implications in cancer therapy; however, poor aqueous solubility limits its utility.<sup>[44–47]</sup> For this reason, innovative strategies for the solubilization and delivery of hydrophobic (or sensitive) drug molecules are required to overcome the physical and biological barriers that hamper therapeutic performance.<sup>[48–53]</sup> Carrier-based approaches for the delivery of PTL have been applied to both lymphoblastic and myeloid leukemias.<sup>[54–56]</sup> Indeed, copolymer-based PTL delivery vectors have been reported to enhance drug bioavailability, showing therapeutic efficacy in vitro and also in vivo, however, the problem of carrier toxicity and producibility still remain.

Herein, we present direct hydration as a powerful tool to obtain drug-loaded PEG-PTMC nanovectors and their successful implementation in the development of a specific ALL therapeutic technology. Through careful optimization of the methodology, highly uniform PEG-PTMC micelles were prepared with a size dictated by their molecular composition (ranging from 20–40 nm). Drug encapsulation, using parthenolide as a pertinent example, was accomplished by codissolution (up to 20 wt% w.r.t. copolymer) in OEG prior to hydration in buffer. Physical characterization, by means of multiple-angle light scattering

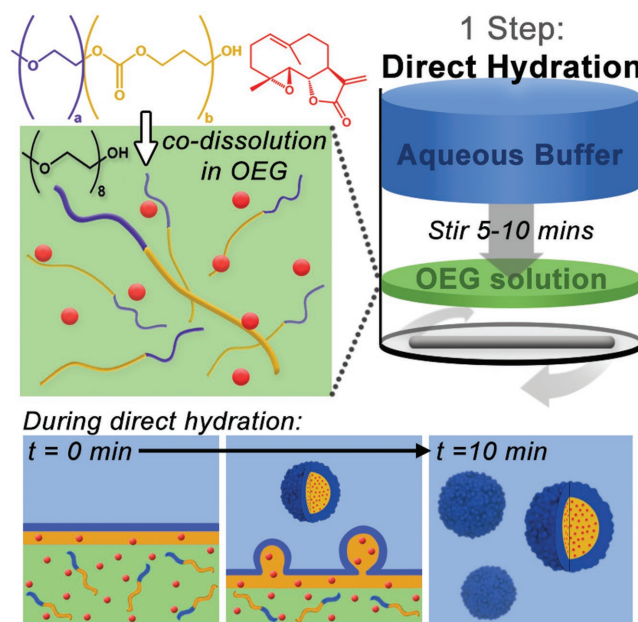


**Figure 1.** Schematic outlining the direct hydration methodology for the production of discrete nanovectors. Codissolution of PEG-PTMC copolymer (chains colored blue and orange, respectively) and drug (red) in OEG (green solvent phase) is followed by stirring with aqueous buffer to create pristine nanovectors in under 10 min, without use of harmful solvents. During direct hydration, as the two phases coalesce, copolymer and drug undergo rapid hydrophobic co-assembly into micellar constructs.

(MALS) and nuclear Overhauser effect spectroscopy (NOESY)  $^1\text{H}$  nuclear magnetic resonance (NMR), confirmed that this process resulted in complete drug encapsulation (within the limits of detection) in discrete nanovectors that required no purification or filtration (**Figure 1**). The resulting nanovectors show excellent nontoxicity toward primary cord blood (CB) cells and, after incorporation of 10 wt% PTL, showed unimpeded cytotoxicity toward both T and B-cell precursor (BCP) ALL patient samples. In particular, it was apparent that the PTL nanovector was less cytotoxic toward CB cells, highlighting the potential of this formulation to actually increase therapeutic efficacy; not only provide a more robust and producible method of formation. We anticipate that the engineering of drug-loaded PEG-PTMC nanovectors, via direct hydration, constitutes a new platform technology for drug delivery that overcomes the problems of control, toxicity, and producibility.

## 2. Results

### 2.1. Evaluation of Copolymer Self-Assembly Using Direct Hydration

Block copolymers comprising varying lengths of PTMC with 1 kDa PEG (Table S1, Supporting Information) were synthesized utilizing the nontoxic organocatalyst methanesulfonic acid according to literature protocols.<sup>[31,32]</sup> For simplicity, PEG-PTMC copolymers are denoted P30, P20, and P15 in relation to their PEG content of 30, 20, and 15 wt%, respectively. This process yielded well-defined copolymers with a polydispersity  $\leq 1.1$ ,

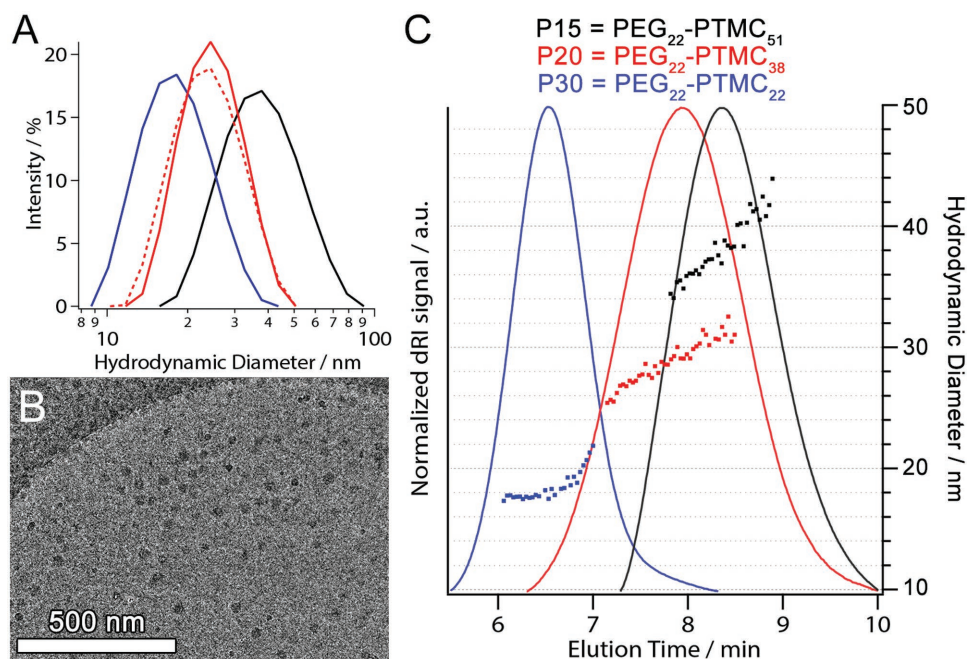


**Figure 2.** Formation of well-defined nanoparticles using direct hydration: A) Intensity size distribution plot for micelles comprising P15 (black), P20 (red), and P30 (blue) prepared via direct hydration (P20 micelles were also prepared by stirring copolymer into buffer directly, red dashes), B) cryo-TEM image of P20 micelles, and C) AF4 data for copolymer micelles with sizes and distributions measured via in-line DLS.

which exist as viscous liquids or waxy solids at room temperature. Self-assembly of PEG–PTMC copolymers was accomplished by dissolution at 50 wt% in viscous OEG ( $M_w = 350$  Da,  $\rho = 1.09$  g mL<sup>-1</sup>) and subsequent hydration through stirring with buffer. No difference in size was observed between copolymer that was directly dissolved into buffer and those prepared by direct hydration (Figure 2A). Nevertheless, it is important to note that direct hydration is vital in the processing of neat (highly viscous/wax-like) PEG–PTMC copolymers due to the importance of drug-loading and ease of handling; which is impossible without OEG dissolution prior to assembly. Cryogenic transmission electron microscopy (cryo-TEM) images of P20 micelles confirmed the presence of spherical nanoscopic constructs, with low electron density (and thereby contrast) owing to their organic nature (Figure 2B). Dynamic light scattering (DLS) yielded average hydrodynamic radii ( $D_h$ ) of 23, 28, and 30 nm for copolymers comprising P30, P20, and P15, respectively, all of which had narrow *pdi* values (<0.1) according to the Zetasizer software. In order to get a more accurate picture of the real size distribution of the micelles we utilized asymmetric flow field-flow fractionation (AF4) coupled with in line DLS (Table S2A, Supporting Information). AF4 is a flow-based separation technique, which can provide unique insight into the structural characteristics of PEG–PTMC micelles, such as a linearly scaled size distribution and shape parameters. AF4 measurements yielded micelle hydrodynamic diameters ( $D_h$ ) of 18–22 (P30), 26–32 (P20), and 34–42 nm (P15) (Figure 2C). Analysis of the ratio between radius of gyration and hydrodynamic radius ( $R_g/R_h$ ), or the particle shape ratio ( $\rho$ ), was performed using AF4-coupled MALS. Although the smallest micelles were below the accepted limit of detection for  $R_g$  (<10 nm),  $\rho$  values of  $\approx 0.8$  were obtained for both P20 and P15

micelles (Figure S3, Supporting Information), confirming their dense, spherical nature in accordance with the literature.<sup>[57]</sup> Zeta-potential measurement of P20 micelles were also performed (in 20× diluted phosphate buffered saline (PBS)) and a value of  $-3 \pm 0.5$  mV was recorded.

## 2.2. Drug Loading and Nanovector Characterization

At this stage we selected the (intermediately sized) P20 micelles in order to evaluate drug loading and in vitro performance. From here on, references to micelle composition will refer to the wt% loading of drug (PTL) in P20 micellar particles rather than copolymer composition. Nanovector preparation through incorporation of PTL into the PEG–PTMC micelles was accomplished by codissolution of drug and copolymer in OEG, prior to hydration (Figure 1). Using this facile methodology we confirmed (using DLS) that the limit of encapsulation was in the region of 20 wt%, with aggregation or drug precipitation evident in a 25 wt% formulation (Figure S4, Supporting Information). Critical micelle concentrations (CMC) of *apo* and PTL nanovectors were measured using the fluorescent probe 8-anilino-naphthalene-1-sulfonic acid (ANS), which detects the presence of hydrophobic microenvironments through an increased fluorescent signal at 480 nm. Using the ANS method, CMC values of  $12 \pm 0.5$  and  $10 \pm 1.4$   $\mu\text{g mL}^{-1}$  ( $\approx 2 \times 10^{-6}$  M) were measured for *apo* and 10 wt% PTL nanovectors, respectively (Figure 3A). In order to demonstrate the scalability of PTL solubilization using direct hydration, a homogenous nanovector dispersion was generated comprising 10 wt% PTL nanovectors up to a [PTL] = 4 mg mL<sup>-1</sup> ( $16.1 \times 10^{-3}$  M), an increase of  $\approx 100$  fold as compared to free drug (Figure 3B).

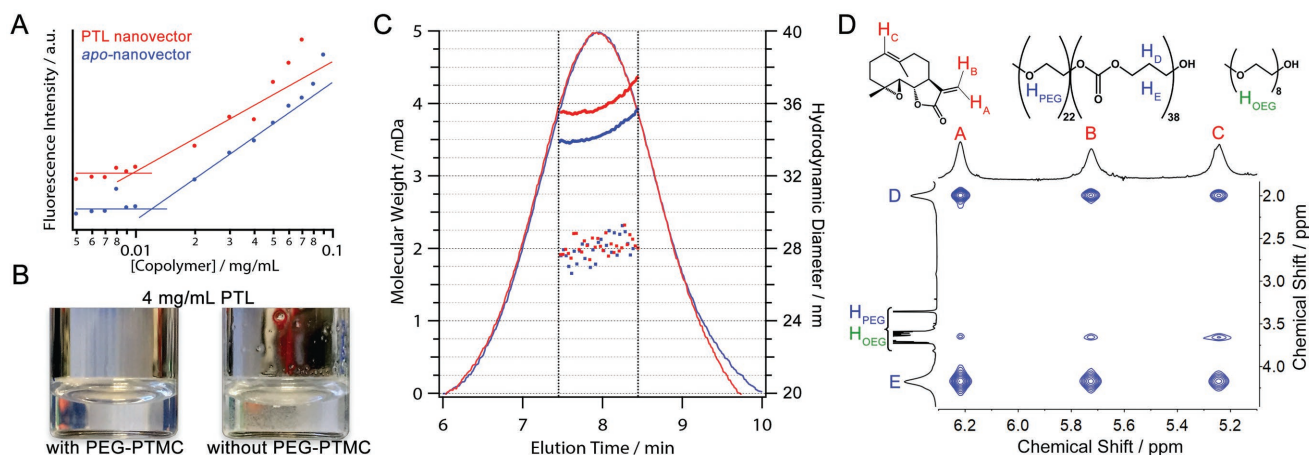


**Figure 3.** PTL nanovector characterization: A) Critical micelle concentration (CMC) determination of *apo*- (blue) and PTL (red) P20 nanovectors via ANS fluorescence, B) images demonstrating the stability of the nanovector formulation at elevated [PTL] as compared to free PTL in solution that undergoes (visible) aggregation, C) AF4-MALS data showing the normalized differential refractive index signals (near-Gaussian traces) and contrasting the hydrodynamic diameter (dots) and molecular weight values (solid lines) of *apo*- (blue) and PTL (red) nanovectors, and D) 2D NMR NOESY data for 10 wt% PTL nanovectors, showing strong spatial correlations between PTL protons (upper) and those of PEG-PTMC (left).

Due to the largely nonaromatic nature of PTL, which renders it chromatically invisible, alternative methodologies are required to evaluate nanovector composition. AF4-MALS/DLS was used to confirm that PTL loading did not have any effect upon the size distribution of the nanovectors; however, an increase in the molecular weight of the particles was observed (Figure 3C). Having measured the refractive index increment ( $dn/dc$ ) for PEG-PTMC as  $0.1027 \pm 0.0008 \text{ mL g}^{-1}$  (Figure S5, Supporting Information), we obtained average values of  $3.62 (\pm 0.1\%)$  and  $4.04 (\pm 0.3\%)$  MDa for *apo* and PTL nanovectors, respectively. From these measurements we can approximate the aggregation number ( $N_{ag}$ ) of the micelles as  $\approx 739$ , which would mean that every chain would occupy in the region of  $3 \text{ nm}^2$  at the hydrated micelle periphery.

$^1\text{H}$  NMR measurements proved to be an excellent counterpart to AF4-MALS for further interrogation of nanovector structure and PTL loading. In particular, 2D NOESY provides spatial information about the microenvironment of any given proton, which can be employed to identify the chemical composition of PTL nanovectors. NMR measurements were performed on 10 wt% PTL-loaded nanovectors, which were directly hydrated into a  $\text{D}_2\text{O}$ -based PBS buffer at a total [PTL] =  $2.75 \text{ mg mL}^{-1}$  ( $11.1 \times 10^{-3} \text{ M}$ ) and measured without any filtration or purification. Cross peaks between PTL protons at 6.27, 5.82, and 5.28 ppm and the core protons of PTMC at 4.16 and 1.99 ppm could only occur if there was long-lasting spatial interaction; indicating that PTL (which exists in a single environment as indicated by the singular nature of the proton resonances) was entirely sequestered in the PEG-PTMC micelles (Figure 3D). Some cross correlation between PTL and ethylene glycol protons was also evident in the 2D spectrum. Closer examination of the NMR data showed correlation between the core protons of PTMC and a broad (27 Hz) signal at 3.65 ppm, rather than the narrow (6 Hz) signal evident in the standard 1D NMR at 3.67 ppm. This was due to correlation between PTMC and coronal PEG protons (broad signal at 3.65 ppm), as opposed to those of OEG (sharp signal at 3.65 ppm) that was free in solution and not present within the micelles (Figure S6, Supporting Information). Indeed, the correlation of PTL in the

2D NMR was with the broad coronal PEG at 3.65 ppm, which can occur due to drug at the core/coronal interface or via a relay signal from the PTMC protons. In addition to NOESY measurements, the  $T_1$  and  $T_2$  relaxation parameters were measured and the results correlated with previous observations. Comparison between the values of free drug protons and loaded drug protons supports the complete encapsulation of PTL.  $T_1$  and  $T_2$  values of protons A and B of PTL decreased by around 50% and 95%, respectively (Table S3, Supporting Information). Lower relaxation times clearly indicate that PTL tumbles more slowly in the nanovector formulation, due to its sequestration inside the dense micelle core.

### 2.3. Stability and Drug Release Characteristics of PTL Nanovectors

To further characterize the physical properties of the nanovector formulation we conducted experiments to determine particle stability, PTL release profile and copolymer stability in PBS and human serum (HS). Standard dosimetry in vivo requires multiple doses of PTL due to its short half-life (in the order of hours),<sup>[58]</sup> which means that particle stability should be evaluated over hours and days. Consistent correlation DLS data of unfiltered samples showed that particles were stable over the course of 6 d in PBS at  $37^\circ\text{C}$  (Figure S7, Supporting Information), which was supported by AF4 (Figure S8, Supporting Information). To confirm particle stability in HS, however, DLS could not be used due to high turbidity. To demonstrate stable drug encapsulation in HS, we engineered Förster (fluorescence) resonance energy transfer (FRET) micelles using the lipophilic fluorescent tracers 3,3'-dioctadecyloxycarbocyanine perchlorate (DiO) and 1,1'-dioctadecyl-3,3',3'-tetramethylindocarbocyanine perchlorate (DiI). DiO/DiI FRET pairing was tailored in the PEG-PTMC system, using direct hydration, to provide a fluorescent read-out that confirms the integrity of discrete nanovectors in complex media, a strategy employed in similar systems.<sup>[59]</sup> Indeed, FRET micelles hydrated into PBS or HS demonstrated equivalent

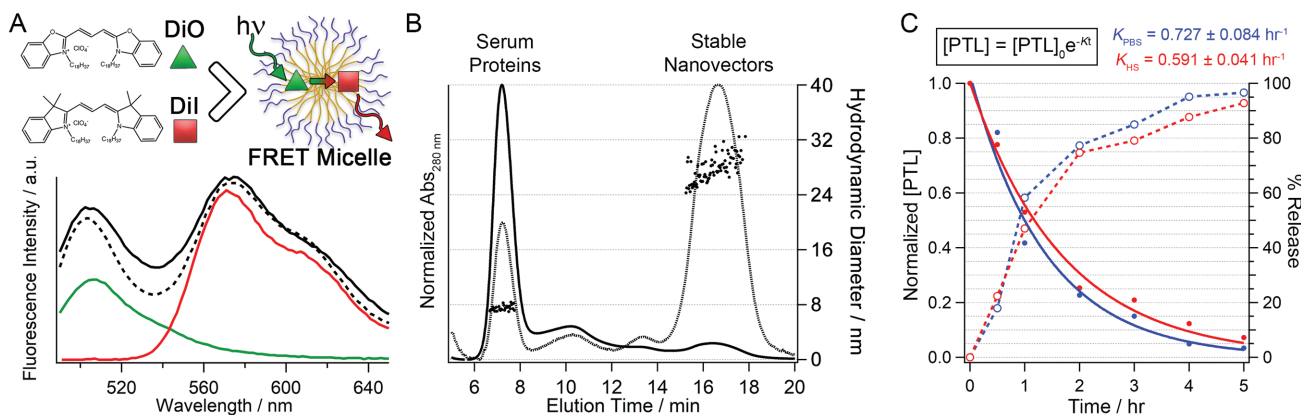


**Figure 4.** Nanovector stability and release characteristics: A) Schematic for the generation of FRET micelles and the fluorescence data showing the normal behavior of DiO (green) or DiI (red) micelles and of FRET micelles hydrated in PBS (dotted line) or HS (solid black line), B) AF4-DLS data for nanovectors after 6 d of incubation in serum at 37 °C with normalized signals for sample absorbance at 280 nm (solid line) and the scattering intensity (dotted line) plotted along with the hydrodynamic diameter (dots), and C) PTL release characteristics of nanovectors in PBS (blue) and serum (red) with the normalized [PTL] (solid symbols and lines) and percentage release data (hollow symbols and dashed line) plotted.

stability with strong FRET signals from DiI at 570 nm, which is of critical importance to the performance of such a system in vitro and in vivo (Figure 4A). In addition, both AF4 measurements, gel permeation chromatography (GPC), and  $^1\text{H}$  NMR were performed on samples that were incubated in HS at 37 °C. Neither the copolymer molecular weight (monitored by GPC retention time and peak width) nor the composition (extracted from the NMR spectra) showed any noticeable change over the course of 6 d (Figure S9, Supporting Information). AF4 also demonstrated the stability of nanovectors in HS after 6 d, with a single population of micelles clearly visible once the serum proteins had been washed away (Figure 4B; Table S2B, Supporting Information). Even after 3 weeks, a discrete population of nanovectors was still visible in samples prepared in PBS and HS, with only a slight increase (1–2 nm) in the  $R_h$  observed during that time (Figure S10, Supporting Information).

The pharmacokinetics of PTL release from nanovectors is an important determinant in their therapeutic performance. Under conditions of dilution similar to those used for in vitro studies (2 mL of PTL nanovector at  $[\text{PTL}] = 0.5 \text{ mg mL}^{-1}$ ,  $2 \times 10^{-3} \text{ M}$ , suspended in 0.6 L buffer), we monitored the [PTL] inside the dialysis bag, and thereby inside the nanovector, by  $^1\text{H}$  NMR (Figure S11, Supporting Information). For both PBS and HS samples, first order drug release was observed ( $[\text{PTL}] = [\text{PTL}]_0 \cdot e^{-Kt}$ ) where  $K = 0.73 \pm 0.08$  and  $0.59 \pm 0.04 \text{ h}^{-1}$ , respectively (Figure 4C). Drug release half times,  $t_{1/2} (= 0.639/K)$  were calculated to be  $0.9 \pm 0.1$  and  $1.1 \pm 0.1 \text{ h}$  for samples in PBS and HS with 90% release being reached after 4–5 h. At double the concentration of nanovectors, and less dilute conditions (30 as compared to 300-fold), the release kinetics of PTL were slowed, with  $K = 0.2 \pm 0.1$  ( $t_{1/2} \approx 4 \text{ h}$ ) and only  $\approx 65\%$  release being reached after 5 h (Figure S12, Supporting Information).

#### 2.4. Performance of PTL Nanovector Against ALL In Vitro

In vitro studies were performed using T- and B-cell precursor ALL patient cells, the latter of which account for the majority of pediatric ALL cases diagnosed (with T-ALL accounting for

$\approx 15\%$ ). CB was used as a normal control and all the patient characteristics are summarized in Table S4 in the Supporting Information. In this work two parameters were varied: (1) the loading of PTL in nanovectors and (2) the overall [PTL] in solution. To ascertain  $\text{IC}_{50}$  values we systematically increased  $[\text{PTL}]_{\text{total}}$  to assess cytotoxicity; however, when comparing nanovectors of different drug loadings the overall [copolymer] varied (e.g., at any given  $[\text{PTL}]_{\text{total}}$ , a 10 wt% nanovector solution contains twice the amount of copolymer, and thereby micelles, as in the 20 wt% nanovector). The performance of PTL nanovectors was compared to free drug, which was added as a dimethylsulfoxide (DMSO) solution to the cells. Although the usage of free PTL can be regarded as a positive control, the necessity to dissolve the compound in organic solvent prevents its use in in vivo application. We therefore wanted to find the optimal nanovector system that performed as well as free PTL, but then at physiologically relevant conditions.

Initially, we compared the effect of PTL loading using PEG-PTMC nanovectors comprising 10 or 20 wt% PTL in single samples. BCP and T-ALL samples for this comparison were selected based on known high PTL resistance, as any increase in cytotoxicity based on PTL loading could be more easily noted. In each sample, using 10 wt% PTL loading, a small increase in cytotoxicity was observed compared to 20 wt% loading; with  $\text{IC}_{50}$  values of 12.28 and  $13.67 \times 10^{-6} \text{ M}$  (CB cells), 9.97 and  $11.91 \times 10^{-6} \text{ M}$  (BCP-ALL, pt. 5), and 9.10 and  $11.10 \times 10^{-6} \text{ M}$  (T-ALL, pt. 2) (Figure 5A). To further evaluate the effect of PTL loading, 2.5, 5, and 10 wt% nanovectors were fabricated and tested against four T-ALL samples, which comprised the PTL resistant (pt. 2) sample and three additional samples that were highly sensitive to PTL. In all four samples, no significant differences in toxicity were observed between formulations, with average  $\text{IC}_{50}$  values of 3.82, 3.57, and  $3.60 \times 10^{-6} \text{ M}$  measured for 2.5, 5, and 10 wt% PTL nanovectors, respectively ( $P \geq 0.94$ , Figure S13, Supporting Information). The higher sensitivity of the additional three T-ALL samples accounts for the drop in  $\text{IC}_{50}$  compared to the 10 wt% nanovectors in pt. 2 ( $9.10 \times 10^{-6} \text{ M}$ ) to the average in all four samples ( $3.60 \times 10^{-6} \text{ M}$ ). All PTL nanovector formulations were equally as effective and showed no

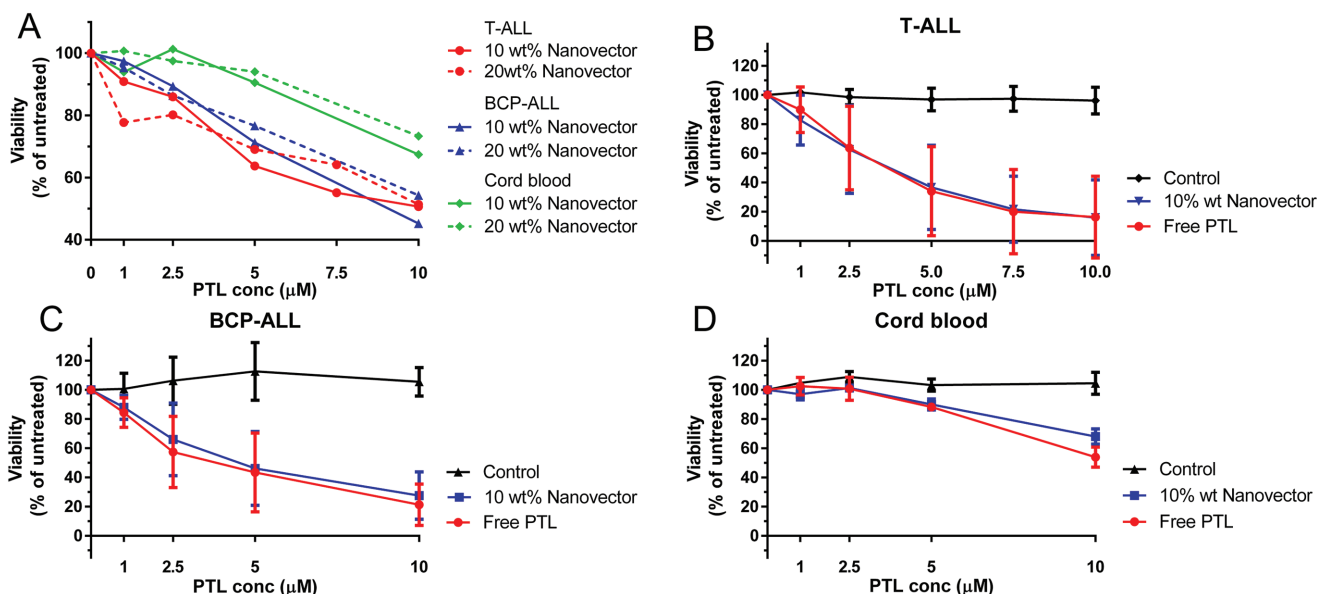


**Figure 5.** In vitro efficacy of PTL Nanovectors against ALL: A) Comparison of cytotoxicity caused by 10 (dotted lines) or 20 (solid lines) wt% PTL nanovectors in a T-ALL, BCP-ALL, and cord blood sample. B–D) Comparison of 10 wt% PTL nanovector (blue line) cytotoxicity versus unloaded nanovector (black line) and free PTL (red line) in primary samples from T-ALL ( $n = 4$ ), BCP-ALL ( $n = 3$ ), and cord blood ( $n = 3$ ). Data represent mean  $\pm$  SD. Results were analyzed by a two-way ANOVA.

significant differences to the toxicity of free PTL dissolved in organic solvent ( $IC_{50}$  of  $3.59 \times 10^{-6}$  M,  $P \geq 0.94$ ). Significantly, apo-nanovectors had no toxic effects on these samples, even at the highest micelle concentrations of  $0.1 \text{ mg mL}^{-1}$ . Consequently, PTL was used at loading weights  $\leq 10$  wt% for all subsequent experiments.

Side-by-side evaluation of 10 wt% PTL nanovectors showed that cytotoxicity was not significantly different between T-ALL and BCP-ALL ( $P \geq 0.8$ ) across all doses and was significantly reduced toward CB cells (Figure 5B–D; Figure S14, Supporting Information). As already stated, 10 wt% PTL nanovector treatment in the four T-ALL samples gave an average  $IC_{50}$  of  $3.60 \times 10^{-6}$  M ( $P = 0.01$ ). For the three BCP-ALL samples tested, an average  $IC_{50}$  of  $4.38 \times 10^{-6}$  M PTL ( $P = 0.02$ ) was obtained with the efficacy of the PTL nanovector being similar to that of free PTL, which had an  $IC_{50}$  of  $3.76 \times 10^{-6}$  M ( $P = 0.79$ ). Again, no toxicity was observed of the apo-nanovector at all concentrations. Concerning CB, treatment with 10 wt% PTL nanovectors showed significantly lower toxicity ( $IC_{50}$   $12.45 \times 10^{-6}$  M PTL) as compared to the effects on BCP-ALL ( $P = 0.02$ ) or T-ALL ( $P = 0.03$ ) cells. Although the effects of PTL nanovectors on CB cells were similar to that of free PTL ( $IC_{50}$   $10.37 \times 10^{-6}$  M) up to  $5 \mu\text{M}$ , at  $10 \times 10^{-6}$  M free PTL was significantly more toxic to these cells ( $P = 0.01$ ). Once again, no toxicity was observed using the apo-nanovector. Apo-nanovector toxicity was also assessed at higher concentrations in CB cells, only at a concentration of  $5 \text{ mg mL}^{-1}$  PEG–PTMC was a small drop in viability observed ( $90 \pm 15\%$ , Figure S15, Supporting Information).

In order to explore the biochemical mechanism of PTL nanovector activity we explored the induction of reactive oxygen species (ROS) stress and inhibition of NF- $\kappa$ B in leukemia cell apoptosis. In all four T-ALL samples, preloaded with the ROS sensitive probe CM- $H_2$ DCFDA, ROS levels significantly

increased when treated with 2.5 ( $11.76 \pm 3.32$  fold), 5 ( $12.32 \pm 1.69$  fold), or 10 wt% ( $11.66 \pm 1.66$  fold) PTL nanovectors and free PTL ( $13.23 \pm 2.88$  fold) compared to untreated cells ( $P \leq 0.03$ ). No significant difference in ROS levels was observed between the cells treated with the various PTL formulations ( $P \geq 0.99$ ) and, as expected, apo-nanovectors showed no significant ROS inducing effects on these samples. (Figure 6A). Phosphorylation of the NF- $\kappa$ B subunit, p65, is an indicator of NF- $\kappa$ B activation, which PTL is known to inhibit. Indeed, phosphorylated p65 expression was significantly reduced in cells treated with either PTL nanovectors ( $13.85 \pm 8.01$  au,  $P \leq 0.0001$ ) or free PTL ( $13.10 \pm 8.61$  au,  $P \leq 0.0001$ ) compared to cells treated with unloaded nanovectors ( $31.76 \pm 15.08$  au) (Figure 6B).

Having demonstrated that PTL is functionally indistinct against ALL cells in vitro when formulated within PEG–PTMC micelles, we assessed the delivery of hydrophobic cargo via the extracellular membrane using a model fluorescent dye. Using fluorescent nanovectors, loaded with 1 wt% DiO, cell uptake could be assessed. T-ALL samples treated with DiO nanovectors at  $37^\circ\text{C}$  showed a mean increase of  $1.58 \pm 0.16$  fold in DiO fluorescence after 30 min of treatment increasing to a maximum of  $2.91 \pm 0.18$  fold increase after 24 h (Figure S16, Supporting Information). Incubating cells with DiO nanovectors at lower temperatures significantly reduced cellular fluorescence, with a  $1.05 \pm 0.02$  ( $P \leq 0.0001$ ) fold increase at  $4^\circ\text{C}$  and  $0.98 \pm 0.08$  ( $P \leq 0.0001$ ) at  $22^\circ\text{C}$  after 3 h, compared to  $2.29 \pm 0.07$  at  $37^\circ\text{C}$  after the same time interval. To directly assess if nanovectors were up-taken via endocytosis in T-ALL cells, Dynasore (a dynamin inhibitor) was applied to samples prior to incubation. Dynamin inhibition resulted in lower fluorescence uptake in cells at all time points analyzed, with a  $1.2 \pm 0.05$  fold increase ( $P \leq 0.0001$ ) in dynamin inhibited cells after 3 h compared to  $2.0 \pm 0.05$  in uninhibited cells. (Figure 6C).

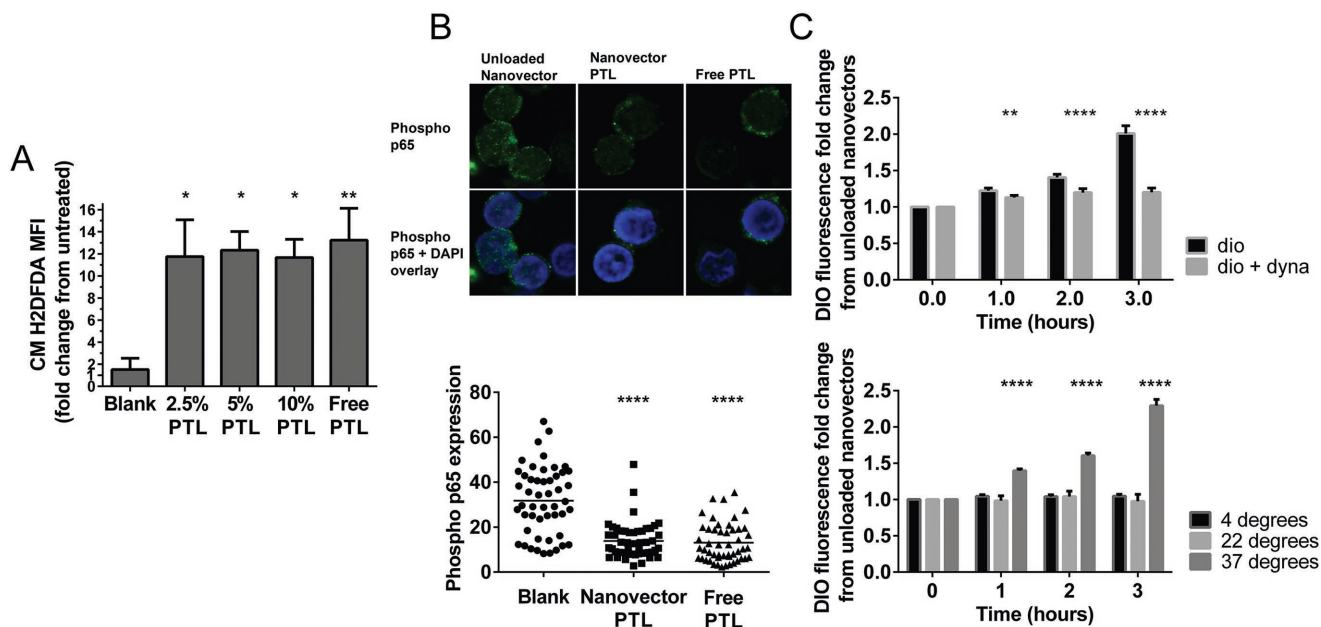


**Figure 6.** Evaluation of PTL nanovector function in vitro: A) Comparison of ROS induction in T-ALL samples by PTL loaded nanovectors (2.5%, 5%, and 10%), free PTL, and unloaded nanovector at a dose of  $10 \times 10^{-6}$  M for 1 h (data expressed as fold change from untreated cells). B) Representative fluorescence image showing the expression of phosphorylated p65 (green fluorescence) in T-ALL cells treated with 10 wt% PTL nanovectors, unloaded nanovectors, or unmodified PTL for 4 h. Expression was quantified in ImageJ in 50 cells from each treatment group. C) Comparison of the uptake of 1 wt% DiO nanovectors in T-ALL samples with or without endocytosis inhibition by Dynasore or under different temperatures during incubation (4, 22, or 37 °C). Data expressed as fold change in DIO fluorescence from unloaded nanovectors. Data represent mean  $\pm$  SD. Results were analyzed by one-way ANOVA.

### 3. Discussion

The utility of direct hydration for the self-assembly of PEG–PTMC copolymers was exemplified by the size control (determined by copolymer composition) and strikingly narrow distributions of the resulting spherical micelles (Figure 2; Figure S3, Supporting Information). These results exemplified the chemical compatibility between OEG and PEG–PTMC, which was sufficiently versatile to facilitate drug (PTL) incorporation in a robust process. Indeed, PTMC was chosen for this research based on observed affinity for direct hydration and its favorable assembly behavior, tending toward the formation of spherical micelles. The ability to codissolve copolymer and drug in OEG and hydrate such well-defined, structurally discrete nanoparticles (reminiscent of the structural uniformity of viruses), in a process that takes less than 10 min, makes this a valuable technological platform.

Evaluation of the physicochemical properties of PTL nanovectors, comprising copolymer P20, yielded maximal drug loadings in the region of 20 wt% (Figure S4, Supporting Information) and CMC values in the low-micromolar regime; at least 100-fold lower than commercial surfactants and amphiphilic copolymers (Figure 3A). By upscaling the formulation to  $[PTL] = 4 \text{ mg mL}^{-1}$  (10 wt% w.r.t. copolymer) we successfully obtained nanovectors without evidence of aggregation (Figure 3B). Thereafter, we wanted to understand if, indeed, the nanovector formulation was as nanoscopically uniform as initial analysis indicated. To that end,  $^1\text{H}$  NOESY NMR and AF4-MALS provided the detailed structural insights necessary. Molecular weight determination, using AF4-MALS, confirmed a

mass increase of  $\approx 10$  wt% and no significant change in micelle size as a result of PTL loading (at 10 wt%, Figure 3C; Figure S5, Supporting Information). To corroborate this, ( $^1\text{H}$ ) 2D NOESY and relaxation time measurements confirmed that (within the detection limits) all drug present in solution was strongly associated with the micelle core (Figure 3D; Table S3, Supporting Information). Moreover, the role of OEG, as a dispersant that does not interact with the resulting nanostructures was also confirmed (Figure S6, Supporting Information). Therefore, we not only present a robust methodology but have demonstrated that the resulting drug nanovectors are, on a nanoscopic level, homogenous and not requiring purification.

As a biodegradable copolymer, PEG–PTMC is known to breakdown under physiological conditions;<sup>[60]</sup> however, it is not well known how this can affect nanoparticles. We observed that PTL nanovectors did not undergo disassembly over the course of 6 d in PBS or HS, as detected by DLS (Figure S7, Supporting Information), FRET measurements (Figure 4A), AF4-DLS (Figure 4B; Figure S8, Supporting Information) or by monitoring copolymer chain integrity (Figure S9, Supporting Information). Extending stability measurements to 3 weeks highlighted the stability of the nanovector platform in both PBS and HS (Figure S10, Supporting Information). An observed increase in the hydrodynamic size of nanovector in HS was likely due to protein adsorption. Interestingly, the utility of AF4 was showcased by the separation from serum proteins from pristine nanovectors in order to directly observe their presence after direct hydration into HS. First order release of PTL (in PBS or HS) from the nanovectors, under dilute dialysis conditions, highlighted the discrete nature of the formulation; where the absence



of a “burst” release indicated a gradual diffusion of uniformly encapsulated cargo (Figure 4C; Figure S11, Supporting Information). Release of 80–90% of drug within 5 h (to an overall [PTL] well below the solubility limit) was not surprising as PTL is known to release more rapidly in contrast to more hydrophobic molecules, such as Nile Red or DiO.<sup>[61]</sup> Repeating release studies under conditions closer to those that would be used in vivo (higher [nanovector] and less dilution), a dramatic reduction in release kinetics was observed, with a fourfold increase in  $t_{1/2}$  (Figure S12, Supporting Information). This highlights that the release of PTL from nanovector occurs as a consequence of PTL diffusion, dictated by the local environment.

In order to demonstrate that this platform technology can be applied to cancer therapy, we have evaluated the efficacy of PTL nanovectors toward ALL. This biodegradable nanovector platform was justified by the exquisite nontoxicity of the *apo*-nanovector toward sensitive patient cell samples; a challenge in developing ALL nanotherapeutics (Figure S14, Supporting Information).<sup>[54,55]</sup> Using up to [PEG–PTMC] = 5 mg mL<sup>-1</sup> no toxicity toward CB cells was observed, demonstrating that biodegradable nanovectors were, indeed, biocompatible (Figure S15, Supporting Information). In vitro assays examining the effect of drug loading, indicated that 2.5–10 wt% PTL nanovectors were equally as effective, with a slight reduction in cytotoxicity at higher loading, contrary to popular thought (Figure 5A; Figure S13, Supporting Information). A key feature of PTL is its reported specificity toward ALL and limited effect upon healthy hematopoietic cells.<sup>[40,43]</sup> Indeed, this behavior was translated to the PTL nanovector platform, which showed excellent cytotoxicity toward a range of T- and BCP-ALL patient samples (Figure 5B,C). Interestingly, we observed that PTL nanovectors were significantly less toxic toward healthy CB cells at  $10 \times 10^{-6}$  M PTL (Figure 5D), which points toward specific therapeutic advantages for this system.

To further evaluate PTL nanovector performance, in vitro, we performed a number of biochemical assays associated with PTL activity; monitoring ROS levels, NF- $\kappa$ B expression, and nanovector uptake.<sup>[43,62]</sup> In agreement with cytotoxicity studies, PTL nanovectors induce ROS and inhibit NF- $\kappa$ B in a similar fashion to free PTL, as opposed to other untargeted systems that can inhibit drug activity (Figure 6A,B). Using an endocytotic inhibitor (Dynasore) we also examined cellular uptake of nanovectors.<sup>[63]</sup> DiO-loaded nanovectors were taken up by T-ALL cells most strongly over the first few hours; however, this continued over the following 24 h (Figure S16, Supporting Information). Nanovector uptake was interrupted both by the cessation of endocytosis or by incubation of cells at lower temperatures, confirming that particle uptake is occurring during the same timescales as in vitro studies (Figure 6C).

## 4. Conclusion

In this work, we have presented a novel methodology for the preparation of biodegradable, drug loaded nanovectors and established their utility in the treatment of ALL in vitro. Direct hydration provides a uniquely facile method for the preparation of well-defined, drug-loaded nanovectors that can be prepared with physical features (such as size) dictated by their chemical

composition. Moreover, such nanovectors possess complete drug encapsulation that justifies direct implementation without purification or postprocessing. Parthenolide, a potent NF- $\kappa$ B inhibitor that has wide-ranging applications in cancer therapy, was effectively incorporated in PEG–PTMC nanovectors and, thereafter, effectively applied toward in vitro studies using ALL patient samples. With excellent biocompatibility of the *apo*-nanovector and specific cytotoxicity of PTL-loaded nanovectors, the potential of this system is clearly demonstrated. We anticipate that this platform can readily be applied to a wide range of drugs and to engineering more complex copolymeric nanosystems for application in cancer therapy; free from the constraints of complex fabrication processes, background toxicity or impeded drug efficacy.

## 5. Experimental Section

**Materials:** All chemicals were used as received unless otherwise stated. For the synthesis of the block copolymers, monomethoxy mPEG<sub>22</sub>-OH (1 kDa) was purchased from Rapp Polymers and trimethylene carbonate from Acros Organics. For in vitro analysis of cells; L-glutamine, penicillin/streptomycin, fetal calf serum, ROS probe CM-H<sub>2</sub>DCFDA, and Hanks balanced salt solution (HBSS) were supplied by Thermo Scientific. Annexin-V-FITC and propidium iodide (PI) were supplied by Miltenyi Biotec. All other chemicals were supplied by Sigma-Aldrich. Ultra-pure MilliQ water obtained from a Labconco Water Pro PS purification system (18.2 M $\Omega$ ) was used for the phosphate buffer solutions. Details of all instrumentation used for particle characterization can be found in the Supporting Information. Paediatric leukemia and normal cord blood samples were obtained with written consent and with approval of University Hospitals Bristol NHS Trust and the National Research Ethics Committee London-Brent.

**Organocatalyzed Synthesis of PEG–PTMC Block Copolymers:** Using a modified literature procedure,<sup>[31]</sup> monomethoxy PEG-OH ( $M_w = 1$  kDa,  $\bar{D} < 1.1$ ) was weighed into a dried round bottom flask (typically 0.1 mmol, 105 mg), to which a stoichiometric amount of trimethylene carbonate was added (either 5.2, 3.8, or 2.2 mmol for copolymers comprising 15, 20, or 30 wt% PEG, respectively). Dry toluene ( $\approx 50$  mL) was then added and evaporated, in order to ensure dryness prior to polymerization. Dried reagents were then dissolved in dry dichloromethane (DCM, 10 mL) and methanesulfonic acid (0.1 mmol = 6.2  $\mu$ L) was added under argon to initiate polymerization. The reaction was stirred at 30 °C for 24 h, until no monomer was observed in the <sup>1</sup>H NMR spectrum (Figure S1, Supporting Information). The reaction mixture was subsequently diluted with DCM and washed with saturated NaHCO<sub>3</sub> then brine before drying over Na<sub>2</sub>SO<sub>4</sub>, concentrated and precipitated into ice cold diethyl ether ( $\approx 100$  mL). After decanting excess ether, the waxy solid was redissolved in dioxane and lyophilized for ease of storage and handling. Yields of 80–90% were obtained with the exact composition determined by <sup>1</sup>H NMR (Figure S2, Supporting Information) and polydispersity determined by gel permeation chromatography (Table S1, Supporting Information).

**Micelle Formation and Drug Encapsulation via Direct Hydration:** PEG–PTMC was dissolved in OEG at 50 wt% at 45 °C with manual mixing to ensure homogeneity. Subsequently, 10  $\mu$ L of this viscous solution was added to the bottom of a 5 mL vial and stirred at 200 rpm with buffer then added up to the desired [copolymer] and left to hydrate for 10 min. Drug encapsulation was accomplished by codissolution of PTL powder into the initial OEG solution at the desired ratio to copolymer without the need for purification. Drug loading was determined with <sup>1</sup>H NMR NOESY and relaxation experiments. Technical details can be found in the Supporting Information.

**CMC Determination:** CMC values for P20 micelles (with and without 10 wt% of PTL) were determined using ANS ( $\lambda_{ex} = 360$  nm/ $\lambda_{em} = 480$  nm). A dilution series was made of the micellar solutions in a multiwell plate (190  $\mu$ L in each well) and 10  $\mu$ L of  $1 \times 10^{-3}$  M ANS

was added to each. Measurements were performed at 37 °C and the fluorescence intensity at 480 nm was used as a read-out.

**Nanovector Stability and Drug Release Studies:** Nanovector stability in both PBS and HS was monitored using DLS, GPC, and AF4 (see the Supporting Information for technical details). In order to monitor drug release and copolymer (P20) stability, 2 mL of 10 wt% PTL nanovector solutions were suspended at a [copolymer] = 5 mg mL<sup>-1</sup> (with [PTL] = 2.2 × 10<sup>-3</sup> M) in a dialysis bag (MWCO 3.5 kDa) within 600 mL of PBS at room temperature. Under conditions of increased concentration, and less dilution, nanovectors at [copolymer] = 10 mg mL<sup>-1</sup> (with [PTL] = 1 mg mL<sup>-1</sup>, 4 × 10<sup>-3</sup> M) were prepared and 8 mL was dialyzed against 250 mL of PBS at room temperature. The nanovector solution was lyophilized at sequential time points, redissolved in CDCl<sub>3</sub> and filtered (0.2 μm PTFE) before measurement by GPC and NMR. To determine PTL content from the <sup>1</sup>H NMR spectra, PTL peaks at 6.3 and 5.6 ppm were normalized against the PTMC peak at 4.2 ppm.

Formation of FRET micelles, to demonstrate stability in human serum, was accomplished using a slight modification to the aforementioned method. Coencapsulation of DiO and Dil was achieved by first dissolving both components in OEG. Thereafter, PEG-PTMC was dissolved into this dye/OEG solution up to [copolymer] = 50 wt% and FRET micelles were prepared via direct hydration (as previously described). Optimal loading of DiO and Dil, where maximal FRET was observed by UV-vis, was found to be 0.06 and 0.247 wt%, respectively.

**PTL Nanovector Cytotoxicity Inducing Cell Death:** For cytotoxicity testing, cells were plated at 2 × 10<sup>5</sup> per mL in RPMI-1640 supplemented medium and treated with PTL nanovectors or free PTL (1–10 × 10<sup>-6</sup> M). Cells were then incubated with drug for 24 h (37 °C, 5% O<sub>2</sub>, 5% CO<sub>2</sub>). After incubation, the cells were washed and resuspended in HBSS containing Annexin-V conjugated to FITC for 10 min at 4 °C in the dark. Cells were then washed, resuspended in HBSS, and stained with PI (1 μg mL<sup>-1</sup>) immediately prior to flow cytometric analysis.

**ROS Induction and Inhibition of NF-κB by PTL Nanovectors:** To test ROS induction, T-ALL cells from four pediatric patients were plated at 2 × 10<sup>5</sup> cells per mL in HBSS containing 2% human serum albumin. Cells were treated with 5 × 10<sup>-6</sup> M of the redox sensitive probe 5-(6)-chloromethyl-2',7'-dichlorodihydrofluorescein diacetate (CM-H<sub>2</sub>DCFDA) for 30 min at 37 °C. Cells were washed and incubated for 1 h with PTL nanovectors (2.5%, 5%, or 10% PTL loading), free PTL (in both cases [PTL]<sub>total</sub> = 10 × 10<sup>-6</sup> M) or apo-nanovector. After treatment cells were washed, resuspended in HBSS, and stained with PI to exclude dead cells immediately prior to flow cytometric analysis. For phosphorylated p65 staining, 5 × 10<sup>4</sup> cells from patient sample 4 were treated with 10 × 10<sup>-6</sup> M PTL (10 wt% PTL loading in nanovectors or free PTL) or unloaded nanovectors for 4 h. During PTL incubation cells were left to settle onto poly-D-lysine coated coverslips. Cells were washed three times in PBS and fixed in 2% paraformaldehyde for 10 min at 4 °C. Cells were washed three times in PBS and treated with staining buffer containing 3% fetal bovine serum (FBS) and 0.1% triton x-100 in PBS for 1 h. Cells were then treated with either rabbit antihuman phospho p65 (pp65, 1:100) or rabbit IgG control (1:100) antibody in staining buffer for 16 h at 4 °C. Cells were washed three times in PBS and treated with goat antirabbit IgG conjugated to alexa fluor 488 (1:100) in staining buffer for 1 h at room temperature (RT) in the dark. Cells were washed three times in PBS and mounted onto slides with prolong gold mounting medium containing DAPI. Cells were imaged on a Leica SP8 AOBs confocal laser scanning microscope.

**Cellular Uptake of Fluorescent (DiO) Nanovector:** To measure nanovector uptake, PEG-PTMC micelles were loaded with 1 wt% DiO in a similar fashion to the DiO/Dil FRET micelles. To assess uptake in T-ALL samples, cells were plated at 2 × 10<sup>5</sup> per mL in RPMI-1640 supplemented medium and treated with nanovectors for up to 24 h. To assess if uptake was blocked by temperature changes, cells were incubated at 37, 22, or 4 °C for 30 min prior to and during nanovector incubation. To assess if uptake was blocked by inhibiting endocytosis via dynamin inhibition, cells were incubated with 80 × 10<sup>-6</sup> M dynasore hydrate for 30 min prior to and during nanovector incubation at 37 °C. After incubation cells were washed and resuspended in HBSS and stained with PI immediately prior to flow cytometric analysis.

## Supporting Information

Supporting Information is available from the Wiley Online Library or from the author.

## Acknowledgements

R.R. and B.C.E. contributed equally to this work. This work was supported by the Dutch Ministry of Education, Culture and Science (Gravitation program 024.001.035), the European Union's Horizon 2020 research and innovation programme Marie Skłodowska-Curie Innovative Training Networks (ITN) Nanomed, under grant No. 676137. In vitro studies were supported by a generous donation from Richard Cunningham and by grants from the Department of Health, the Wellcome Trust Institutional Strategic Support Fund, Elizabeth Blackwell Institute, University of Bristol. The authors wish to thank the consultants and oncology staff at Bristol Royal Hospital for Children. The authors are grateful to the patients and their families who gave permission for their cells to be used for research. The authors thank the EPSRC (Early Career Fellowship EP/K026720/1) for support of A.W.P. The authors thank the Ser Cymru II programme for support of D.S.W.; this project received funding from the European Union's Horizon 2020 research and innovation programme under the Marie Skłodowska-Curie grant agreement No 663830.

## Conflict of Interest

The authors declare no conflict of interest.

## Keywords

acute leukemia, drug delivery, nanomedicine, parthenolide, self-assembly

Received: October 30, 2017

Revised: January 20, 2018

Published online: July 12, 2018

- [1] W. R. Sanhai, J. H. Sakamoto, R. Canady, M. Ferrari, *Nat. Nanotechnol.* **2008**, *3*, 242.
- [2] K. Riehemann, S. W. Schneider, T. A. Luger, B. Godin, M. Ferrari, H. Fuchs, *Angew. Chem., Int. Ed.* **2009**, *48*, 872.
- [3] R. A. Petros, J. M. DeSimone, *Nat. Rev. Drug Discovery* **2010**, *9*, 615.
- [4] A. Albanese, P. S. Tang, W. C. W. Chan, *Ann. Rev. Biomed. Eng.* **2012**, *14*, 1.
- [5] N. P. Truong, M. R. Whittaker, C. W. Mak, T. P. Davis, *Expert Opin. Drug Delivery* **2015**, *12*, 129.
- [6] J. I. Hare, T. Lammers, M. B. Ashford, S. Puri, G. Storm, S. T. Barry, *Adv. Drug Delivery Rev.* **2017**, *108*, 25.
- [7] V. J. Venditto, F. C. Szoka, *Adv. Drug Delivery Rev.* **2013**, *65*, 80.
- [8] N. Nishiyama, Y. Matsumura, K. Kataoka, *Cancer Sci.* **2016**, *107*, 867.
- [9] B. L. Banik, P. Fattahi, J. L. Brown, *Wiley Interdiscip. Rev.: Nanomed. Nanobiotechnol.* **2016**, *8*, 271.
- [10] A. Gothwal, I. Khan, U. Gupta, *Pharm. Res.* **2016**, *33*, 18.
- [11] Z. Tang, C. He, H. Tian, J. Ding, B. S. Hsiao, B. Chu, X. Chen, *Prog. Polym. Sci.* **2016**, *60*, 86.
- [12] Y. Mai, A. Eisenberg, *Chem. Soc. Rev.* **2012**, *41*, 5969.
- [13] G. Gaucher, M.-H. Dufresne, V. P. Sant, N. Kang, D. Maysinger, J.-C. Leroux, *J. Controlled Release* **2005**, *109*, 169.
- [14] A. Blanz, S. P. Armes, A. J. Ryan, *Macromol. Rapid Commun.* **2009**, *30*, 267.
- [15] G. E. Luckachan, C. K. S. Pillai, *J. Polym. Environ.* **2011**, *19*, 637.

- [16] H. Tian, Z. Tang, X. Zhuang, X. Chen, X. Jing, *Prog. Polym. Sci.* **2012**, *37*, 237.
- [17] K. Fukushima, *Biomater. Sci.* **2016**, *4*, 9.
- [18] N. Kamaly, B. Yameen, J. Wu, O. C. Farokhzad, *Chem. Rev.* **2016**, *116*, 2602.
- [19] P. P. Wibroe, D. Ahmadvand, M. A. Oghabian, A. Yaghmur, S. M. Moghimi, *J. Controlled Release* **2016**, *221*, 1.
- [20] M. Beck-Broichsitter, J. Nicolas, P. Couvreur, *Eur. J. Pharm. Biopharm.* **2015**, *97*, 304.
- [21] L. Tang, X. Yang, Q. Yin, K. Cai, H. Wang, I. Chaudhury, C. Yao, Q. Zhou, M. Kwon, J. a. Hartman, I. T. Dobrucki, L. W. Dobrucki, L. B. Borst, S. Lezmi, W. G. Helferich, A. L. Ferguson, T. M. Fan, J. Cheng, *Proc. Natl. Acad. Sci. USA* **2014**, *111*, 15344.
- [22] S. Shah, Y. Liu, W. Hu, J. Gao, *J. Nanosci. Nanotechnol.* **2011**, *11*, 919.
- [23] P. Decuzzi, B. Godin, T. Tanaka, S.-Y. Lee, C. Chiappini, X. Liu, M. Ferrari, *J. Controlled Release* **2010**, *141*, 320.
- [24] C. LoPresti, H. Lomas, M. Massignani, T. Smart, G. Battaglia, *J. Mater. Chem.* **2009**, *19*, 3576.
- [25] P. Decuzzi, R. Pasqualini, W. Arap, M. Ferrari, *Pharm. Res.* **2009**, *26*, 235.
- [26] S. Mitrageotri, J. Lahann, *Nat. Mater.* **2009**, *8*, 15.
- [27] S. E. A. Gratton, P. A. Ropp, P. D. Pohlhaus, J. C. Luft, V. J. Madden, M. E. Napier, J. M. DeSimone, *Proc. Natl. Acad. Sci. USA* **2008**, *105*, 11613.
- [28] C. P. O'Neil, T. Suzuki, D. Demurtas, A. Finka, J. a. Hubbell, *Langmuir* **2009**, *25*, 9025.
- [29] X. Sui, P. Kujala, G.-J. Janssen, E. de Jong, I. S. Zuhorn, J. C. M. van Hest, *Polym. Chem.* **2015**, *6*, 691.
- [30] Z. Zhang, R. Kuijter, S. K. Bulstra, D. W. Grijpma, J. Feijen, *Biomaterials* **2006**, *27*, 1741.
- [31] D. Delcroix, B. Martín-Vaca, D. Bourissou, C. Navarro, *Macromolecules* **2010**, *43*, 8828.
- [32] N. E. Kamber, W. Jeong, R. M. Waymouth, R. C. Pratt, B. G. G. Lohmeijer, J. L. Hedrick, *Chem. Rev.* **2007**, *107*, 5813.
- [33] X. Jiang, H. Xin, X. Sha, J. Gu, Y. Jiang, K. Law, Y. Chen, L. Chen, X. Wang, X. Fang, *Int. J. Pharm.* **2011**, *420*, 385.
- [34] X. Ke, D. J. Coady, C. Yang, A. C. Engler, J. L. Hedrick, Y. Y. Yang, *Polym. Chem.* **2014**, *5*, 2621.
- [35] S. P. Hunger, C. G. Mullighan, *N. Engl. J. Med.* **2015**, *373*, 1541.
- [36] H. Inaba, M. Greaves, C. G. Mullighan, *The Lancet* **2013**, *381*, 1943.
- [37] A. Redaelli, B. L. Laskin, J. M. Stephens, M. F. Botteman, C. L. Pashos, *Eur. J. Cancer Care* **2005**, *14*, 53.
- [38] C. Prucker, A. Attarbaschi, C. Peters, M. N. Dworzak, U. Pötschger, C. Urban, F.-M. Fink, B. Meister, K. Schmitt, O. a Haas, H. Gadner, G. Mann, *Leukemia* **2009**, *23*, 1264.
- [39] J. Long, Y.-H. Ding, P.-P. Wang, Q. Zhang, Y. Chen, *Tetrahedron Lett.* **2016**, *57*, 874.
- [40] M. L. Guzman, R. M. Rossi, L. Karnischky, X. Li, D. R. Peterson, D. S. Howard, C. T. Jordan, *Blood* **2005**, *105*, 4163.
- [41] J. Wen, K.-R. You, S.-Y. Lee, C.-H. Song, D.-G. Kim, *J. Biol. Chem.* **2002**, *277*, 38954.
- [42] A. J. Steele, D. T. Jones, K. Ganeshaguru, V. M. Duke, B. C. Yogashangary, J. M. North, M. W. Lowdell, P. D. Kottaridis, A. B. Mehta, A. G. Prentice, A. V Hoffbrand, R. G. Wickremasinghe, *Leukemia* **2006**, *20*, 1073.
- [43] P. Diamanti, C. V Cox, J. P. Moppett, A. Blair, *Blood* **2013**, *121*, 1384.
- [44] A. García-Piñeres, M. Lindenmeyer, I. Merfort, *Life Sci.* **2004**, *75*, 841.
- [45] C. H. Lee, Y.-T. Jeon, S.-H. Kim, Y.-S. Song, *BioFactors* **2007**, *29*, 19.
- [46] V. Baud, M. Karin, *Nat. Rev. Drug Discovery* **2009**, *8*, 33.
- [47] M. R. Orofino Kreuger, S. Grootjans, M. W. Biavatti, P. Vandenamee, K. D'Herde, *Anti-Cancer Drugs* **2012**, *23*, 1.
- [48] R. Duncan, R. Gaspar, *Mol. Pharm.* **2011**, *8*, 2101.
- [49] L. Yaling, J. Tan, A. Thomas, D. Ou-Yang, V. R. Muzykantor, *Ther. Delivery* **2012**, *3*, 181.
- [50] Y. H. Yun, B. K. Lee, K. Park, *J. Controlled Release* **2015**, *219*, 2.
- [51] A. Wicki, D. Witzigmann, V. Balasubramanian, J. Huwyler, *J. Controlled Release* **2015**, *200*, 138.
- [52] E. Blanco, H. Shen, M. Ferrari, *Nat. Biotechnol.* **2015**, *33*, 941.
- [53] D. S. Williams, I. A. B. Pijpers, R. Ridolfo, J. C. M. van Hest, *J. Controlled Release* **2017**, *259*, 29.
- [54] R. C. Deller, P. Diamanti, G. Morrison, J. Reilly, B. Ede, R. M. Richardson, K. Le Vay, A. M. Collins, A. Blair, A. W. Perriman, *Mol. Pharm.* **2017**, *14*, 722.
- [55] M. P. Baranello, L. Bauer, C. T. Jordan, D. S. W. Benoit, *Cell. Mol. Bioeng.* **2015**, *8*, 455.
- [56] H. Zong, S. Sen, G. Zhang, C. Mu, Z. F. Alabayati, D. G. Gorenstein, X. Liu, M. Ferrari, P. A. Crooks, G. J. Roboz, H. Shen, M. L. Guzman, *Leukemia* **2016**, *30*, 1582.
- [57] M. Wagner, M. J. Barthel, R. R. A. Freund, S. Hoepfner, A. Traeger, F. H. Schacher, U. S. Schubert, *Polym. Chem.* **2014**, *5*, 6943.
- [58] Z.-J. Yang, W.-Z. Ge, Q.-Y. Li, Y. Lu, J.-M. Gong, B.-J. Kuang, X. Xi, H. Wu, Q. Zhang, Y. Chen, *J. Med. Chem.* **2015**, *58*, 7007.
- [59] S. Lee, J. Y. Tyler, S. Kim, K. Park, J. Cheng, *Mol. Pharm.* **2013**, *10*, 3497.
- [60] J. Yang, W. Tian, Q. Li, Y. Li, A. Cao, *Biomacromolecules* **2004**, *5*, 2258.
- [61] M. P. Baranello, L. Bauer, D. S. W. Benoit, *Biomacromolecules* **2014**, *15*, 2629.
- [62] S. Pei, M. Minhajuddin, K. P. Callahan, M. Balys, J. M. Ashton, S. J. Neering, E. D. Lagadinou, C. Corbett, H. Ye, J. L. Liesveld, K. M. O'Dwyer, Z. Li, L. Shi, P. Greninger, J. Settleman, C. Benes, F. K. Hagen, J. Munger, P. A. Crooks, M. W. Becker, C. T. Jordan, *J. Biol. Chem.* **2013**, *288*, 33542.
- [63] T. Kirchhausen, E. Macia, P. H. E. *Methods Enzym.* **2008**, *438*, 77.